Risk Based Assessment of the Effect of AAR on Shear Walls Strength

NEA/CSNI Benchmark ASCET Phase II Workshop

Task 3-A

December 2017

by

Victor E. Saouma
Mohammad A. Hariri-Ardebili

University of Colorado, Boulder

Contents

List of Figures

List of Tables

1 Introduction

Increasingly engineers are confronted with the need to perform predictive structural assessment based on limited or incomplete data set. This may include damage up to failure assessment (in the context of so-called performance based engineering), or round robin benchmarks. As such deterministic analyses are of limited predictive values, and a probabilistic-based methodology is necessary.

This paper focuses on the development of a methodology for such assessment, and is believed to be the first such contribution in the context of structural failure following alkali silica reaction (ASR) induced expansion. As a vehicle for such an application, the round-robin benchmark surrounding the shear failure of a reinforced concrete wall having suffered from ASR expansion is used. However, for reasons explained later, the authors believe that the reported experimental data may not be of sufficient reliability, and hence the predictive nature of the analysis is reported but deemphasized.

1.1 Background

Though AAR has been known ot affect numerous structures, dams in particular (ICOLD Bulletin 79, 1991) (Amberg, 2011), only recently has it been found in one or more nuclear containment structures (Saouma, 2013a). Despite the lack of publicity, some nuclear power plants reactors are starting to show signs of ASR, (ibid.). In Japan, the (reinforced concrete) turbine generator foundation at Ikata No. 1 NPP (owned by Shihoku Electric Power) exhibits ASR expansion and has thus been the subject of many studies. Takatura et al. (2005a) reports on the field investigation work underway: location, extent of cracking, variation in concrete elastic modulus and compressive strength, expansion in sufficient detail to adequately understand the extent of damage. The influence of ASR on mechanical properties (in particular, the influence of rebar) and on structural behavior has been discussed by Murazumi et al. (2005a) and Murazumi et al. (2005b), respectively. In the latter study, beams made from reactive concrete were tested for shear and flexure. These beams were cured at 40°C and 100% relative humidity for about six weeks. Some doubt remains, however, as to how representative such a beam is for those NPP where ASR has been occurring for over 30 years. A study of the material properties introduced in the structural analysis was first reported by Shimizu et al. (2005b). An investigation of the safety margin for the turbine generator foundation has also been conducted (Shimizu et al., 2005a). Moreover, vibration measurements and simulation analyses have been performed (Takatura et al., 2005b). Takagkura et al. (2005) has recently reported on an update of the safety assessment at this NPP. In Canada, Gentilly 2 NPP is known to have suffered ASR (Orbovic, 2011). An early study by Tcherner and Aziz (2009) actually assessed the effects of ASR on a CANDU^{TM}6 NPP (such as Gentilly 2). In 2012 however, following an early attempt to extend the life of Gentilly 2 until 2040 (with an approx. $1.9B overhaul), Hydro-Quebec announced its decommissioning after 29 years for economic reasons. Yet, as late as 2007, it was reported that *to date, no incidences of ASR-related damage have been identified in U.S. nuclear power plants* (Naus, 2007).

In light of this potential problem which may affect numerous NCS, various research projects were put in place. The Department of Energy is sponsoring large scale mockup tests to assess the effect of confinement on ASR expansion (Le Pape, Y. and Ma, Z. and Cabage, J. and Lenarduzzi, R., 2014). The Nuclear regulatory commission (NRC) has entered into an interagency agreement with the National Institute of Science and Technology to conduct a multi-million dollars research program on the structural performance of nuclear power plants affected by ASR ($5.67M) (NRC-NIST Project, 2014). NRC is also funding a grant and cooperative agreement with the university of Colorado to also assess the effect of ASR on the shear strength deterioration and for the integrity assessment of a NCS suffering from ASR subjected to seismic loading ($653k) (NRC-CU Grant, 2014). Finally, Nextera has funded a major research program at the University of Texas to assess again the effect of ASR on the shear strength of concrete (ADAMS Accession No. ML 121160422, 2012). Similar effort have been undertaken abroad. Most notably in Canada through funding from the Canadian Nuclear Safety Commission (CNSC) (Orbovic et al., 2015) where shear wall affected by ASR have been tested (and whose analyses are reported below). Finally, a major project on the same theme was recently initiated in France (Marquié, 2016) through support from the ISRN.

In terms of related numerical simulations, the authors have investigated the shear response of nuclear containement panels (Saouma, V.E. and Hariri-Ardebili, M. and Puatsananon, W. and Le Pape, Y., 2014) (Saouma, Hariri-Ardebili, and Le Pape, 2015) (Hariri-Ardebili, Saouma, and LePape, 2016) (Saouma et al.,

2016) and thus this work constitutes a natural extension of past analyses combined with the separately developed methodology for probabilistic assessment (Hariri-Ardebili and Saouma, 2016a) (Hariri-Ardebili and Saouma, 2016b).

1.2   Objective

Through the auspices of the OECD, a project for the Assessment of Structures subject to Concrete Pathologies (ASCET) was setup with one of its objective the organization of a blind simulation benchmark to predict the behavior of structural elements with ASR. The selected structure was the shear wall previously tested at the University of Toronto, (Habibi et al., 2015). Participants were given the opportunity to calibrate their models through the first phase (I) of the project where experimental data after 8 months was made available, and asked to submit their numerical prediction for the wall responses (with and without ASR) after 30 months of swelling.

Though the primary objective of this paper is not to merely "compete" in the benchmark study but to introduce an innovative paradigm for investigation. Nevertheless, this paper will try to adhere in as much as possible with the spriti of the benchmark round-robin.

2   Test Description

Based on the provided information, the tested shear wall are shown in Fig. 1 while Fig. 2 shows the corresponding dimensions. The 10M and 20M reinforcements have cross-sectional areas of 100 and 200 mm^2, yield stresses of 430 and 465 MPa, and elastic moduli of 182,000 and 190,000 MPa respectively.
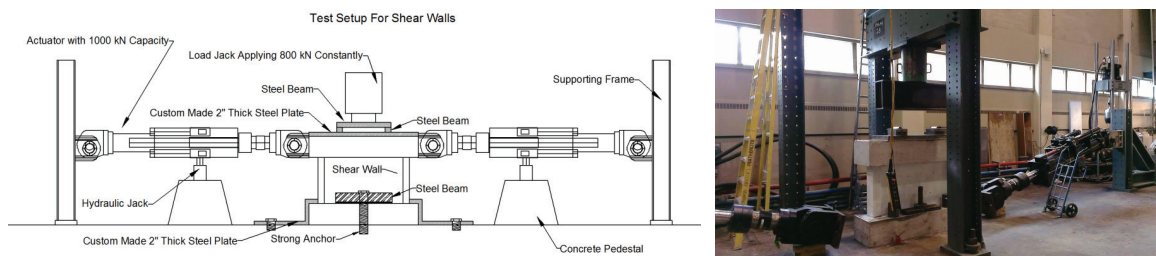
Figure 1: Test setup for the shear wall (Habibi et al., 2015)

In the experiment, a constant vertical force of 800 kN is applied through a 2" spreader beam, and the wall is subjected to a reverse cyclic pushover displacement.

A total of three walls were cast, one without AAR (SW) and two others with AAR (SW-260 and SW-1000). The first two were tested about 240 days after casting and the results made available for calibration. The third wall was tested about 1,000 days after casting and participants in the benchmark round robin were asked to make predictions. The reported mechanical properties are themselves shown in Table 1 and ASR expansions in Table 2.

Table 1: Reported mechanical properties of concrete

Specimen	Age	f_c' (MPa)	f_t' (MPa)	G_F (N/m)	f_r (MPa)	E (MPa)
SW	$\sim$ 240 days	79.0	4.76	179.3	7.26	47,150
SW-260	$\sim$ 260 days	63.7	3.24	120.2	4.64	35,750

Table 2: Reported concrete expansions at 50°C

Days	0	7	28	90	150	180	250
Reactive	0	0.0099	0.0332	0.1115	0.1399	0.1519	0.1850
Non reactive	0	0.0181	0.0249	0.0264	0.0309	0.0329	0.0332
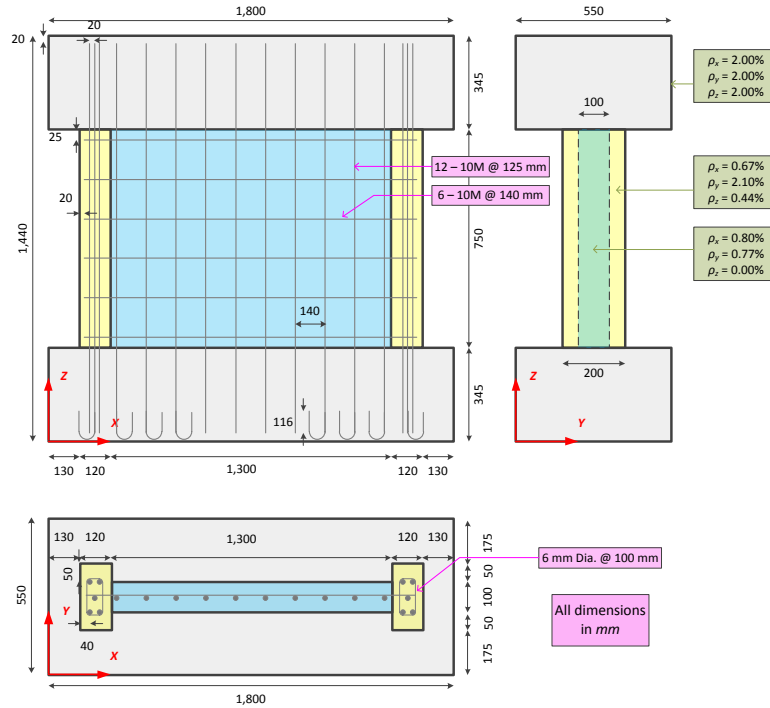
Figure 2: Dimensions of the shear wall

Results of the three tests are summarized in Table 3, and in Fig. 3. It should be noted that the peak loads with and without ASR expansion are 1,354 and 1,180 (SW-260 and SW) or 14% difference, Fig. 3(c). This is a relatively small change, and given the uncertainties in measurement that difference may not be entirely attributed to the effect of expansion.

Table 3: Reported experimental results

Test	Reactive	Age [days]	Peak +ve		Peak -ve		Failure	
			Cap.	Def.	Cap.	Def.	Axial Cap.	Def.
SW	No	~240	990 kN	6.9 mm	1,180 kN	5.6 mm	210 kN	8.2 mm
SW-260	Yes	~260	1,304.9 kN	5.1 mm	1,354 kN	5.1 mm	225 kN	7.1 mm
SW-1000	Yes	~ 1,000	To be predicted by simulation					

3 Modeling Approach

It is argued that numerical simulations can be of different nature:

1. An inconsequential analysis where results are simply to meet basic engineering common sense expectations.

2. *Post-mortem* simulation where one has the luxury to fine-tune/calibrate a model until near exact results are obtained (which is nearly alway possible, irrespective of the model accuracy).

3. Predictive analysis for the future response of a structure.

4. Blind simulation benchmark of an experimental test.

(a) SW   (b) SW-260   (c) Envelope comparison
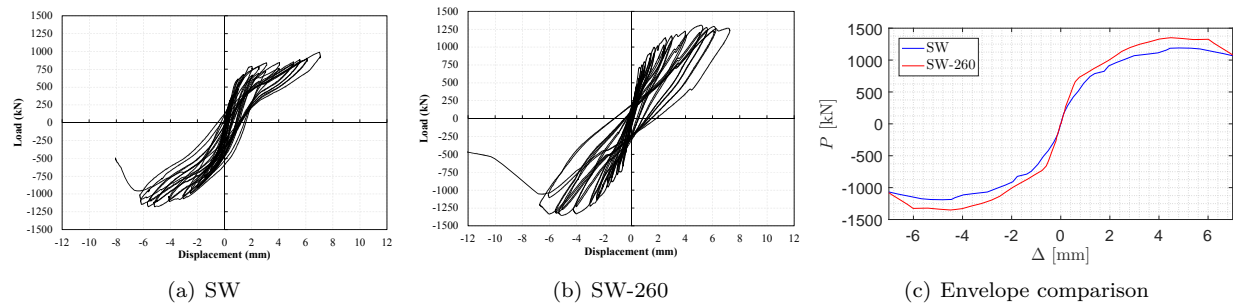
Figure 3: Force displacement results for the first set of walls after 8 months, adapted from (Habibi et al., 2015)

In the context of this last simulation, the numerical modeling may indeed be the simplest part as the real complexity stems from two major unknowns:

Experimental How accurately was the test performed, how credible are the results, are the reported results sufficiently clear and unambiguous? are we checking the model or the test?

Numerical Can one perform a single deterministic and predictive analysis, or should not a probabilistic-based analysis be more appropriate given the epistemic nature of the uncertainties?

The current benchmark study does allow calibration (level 2 above) and requires prediction of known results (level 4). As to the two level of uncertainties (experimental and numerical), those are separately addressed below.

3.1 Experimental Uncertainties

Given the predilection of some to compare experiments and simulations to the third decimal place, and as many feel unsatisfied if results are not within 10-15% (a perfectly honorable place), it is of paramount importance that the results reported by a benchmark organizer be well understood.

In this present context, More specifically, An important question is how are the reported measurements recorded? whereas the load can only be recorded by the (hopefully calibrated) load-cell, how about the displacements? Is the laterally imposed displacement driven by the actuator stroke? how about the displacement associated with the load displacement hysteresis curve? does it account for some "slack" that undoubtedly exist in such a setup? is it directly recorded as the differential between the top and lower beams? how?

Attempts to elucidate these questions with the experimentalist yielded the communication found in Appendix A. As the senior author has indeed much experience in analogous testing, he felt uncomfortable about the reliability of the reported displacements, specially that a spreadsheet with all recorded values (for SW and SW-260) was not provided.

Recalling that Einstein purportedly (and infamously) said

You make experiments and I make theories. Do you know the difference? A theory is something nobody believes, except the person who made it. An experiment is something everybody believes, except the person who made it.

the authors would paraphrase by stating:

You make an experiment, and I make a simulation. I do not fully trust your experiment, neither do I trust a single deterministic analysis. So let us go to Monte-Carlo!

3.2 Epistemic Uncertainties

Simply put, epistemic uncertainties are those caused by an incomplete knowledge of the exact material properties (Der Kiureghian and Ditlevsen, 2009). Given that a nonlinear constitutive model for concrete

contains numerous variables, most of which not provided or even measurable, a two prone approach should be followed:

1. **Sensitivity analysis** to determine to which of the many variables, the shear wall model is most sensitive.

2. **Uncertaintly analysis** after selection of the most sensitive parameters, perform a Monte-Carlo simulation to provide a probabilistic estimate of the prediction.

this approach was recently followed by the authors for the analysis of a major bridge suffering from ASR (Hariri-Ardebili and Saouma, 2016b).

4   Data Preparation

The analysis hinges on two constitutive models: one for the concrete nonlinearity (a fracture-plasticity "smeared crack" model) (Cervenka and Papanikolaou, 2008), and the other for the ASR (Saouma, 2013b). Both have been implemented in the authors finite element code (Saouma, Červenka, and Reich, 2010), and most importantly validated in accordance with the RILEM TC 259 report (Saouma et al., 2017).

4.1   Concrete Smeared Crack Model

The smeared crack model has a total of 12 variables, Table 4. The table not only lists the mean values, but the authors best estimates for the coefficients of variation as well as the lower and upper bonds for uncertainty quantification, and minimum-maximum for the sensitiveness analysis. Also shown are the final outcome as to those retained random variables in each case.

In all analyses, random variables are assumed to have a normal distributional model (leading to maximum entropy) with mean and COV shown in the table. However, those values were subsequently adjusted since the distribution was truncated, Fig. 4.
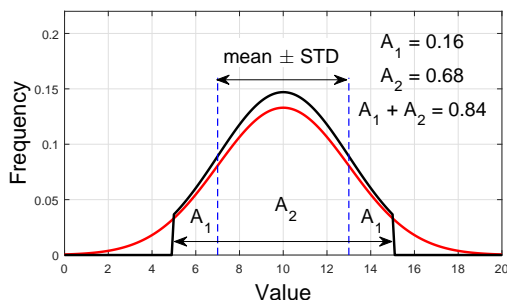
Figure 4: Truncation of normal distribution model and bounds

4.2   Reinforcement and Bond-Slip

The material properties for the reinforcement (either in web and columns or in the beams) were shown in Sec. 2. Though reinforcement properties exhibit little if any epistemic uncertainty, the approach taken was to reduce the area of the reinforcement crossing the beam-column (or beam-web) intersection to account for possible bond-slip. As such, the cross sectional area was arbitrarily reduced by 20% and treated as the only steel variable in the uncertainty quantification analysis.

4.3   ASR Expansion

4.3.1   Model

Proper modeling of the ASR expansion is of paramount importance to this study, and as such has received great scrutiny. The adopted AAR model is described in Appendix B, where the kinetics of the expansion is

Table 4: Material parameters used in numerical simulations

Characteristics	Symbol	Unit	SA	UQ	Mean	COV$_{UQ}$	[LB, UB]$_{UQ}$	[min, max]$_{SA}$
Smeared crack model								
Mass density	ρ	Gg/m^3	0	0	0.00244	-	-	-
Thermal expansion coefficient	α	1/^{o}C	0	0	9.9e-6	-	-	-
Modulus of elasticity*	E	MPa	1	1	47,150	0.2	[28,290 66,010]	[23,575 70,725]
Poisson's ratio	ν	-	0	0	0.2	-	-	-
Tensile strength*	f_t	MPa	1	1	4.76	0.2	[2.86, 6.66]	[2.38, 7.14]
Exponential softening*	G_F	MN/m	1	1	1.79e-4	0.2	[1.08e-4, 2.51e-4]	[8.95e-5, 2.68e-4]
Compressive strength*	f_c	MPa	1	1	-79.0	0.2	[-110.6, -47.4]	[-118.5, -39.5]
Compressive critical displacement	w_d	m	1	0	-5e-4	-	-	[-7.5e-4, -2.5e-4]
Factor for return direction	β	-	1	0	0.50	-	-	[0.25, 1.0]
Factor for roundness of failure surface	e	-	1	0	0.55	-	-	[0.5, 1.0]
Onset of nonlinearity in compression	f_{c0}	MPa	1	0	-20	-	-	[-30, -10]
Plastic strain at compressive strength	ϵ_{cp}	-	1	0	-1e-3	-	-	[-2e-3, -5e-4]
Reinforcement								
Yield stress of main rebar (vertical and horizontal)	f_y^R	MPa	1	0	430	-	-	[215, 645]
Yield stress of main stirrups	f_y^S	MPa	1	0	430	-	-	[215, 645]
Yield stress of crossing rebar	f_y^{R-Cr}	MPa	1	0	430	-	-	[215, 645]
Modulus of elasticity of crossing rebar	E^{R-Cr}	MPa	1	0	182,000	-	-	[91000, 273000]
Cross sectional area of crossing rebar	A_r^{R-Cr}	m^2	1	1	8e-5	-	[4.8e-5, 1e-4]	[6e-5, 1e-4]

* Reported values (Table 3).

given by Eq. 1 and 3 while the degradation in Eq. 4. Those two equations define what will be the variables associated withe the uncertainty quantification (they were not considered in the sensitivity analysis):

τ_L Latency time, Eq. 1 and 3
τ_C Characteristic time, Eq. 1 and 3
ε^∞ Maximum AAR expansion, Eq. 1
U_L Activation energy of the latency time, Eq. 3
U_C Activation energy of the characteristic time, Eq. 3
β_E Residual elastic modulus at the end of the reaction, Eq. 4
β_{ft} Residual tensile strength at the end of the reaction, Eq. 4

Warning it should be emphasized that whereas in this exercise the entire wall will be assigned the same expansion as the one observed from laboratory specimens, this is not exactly valid. There is ample evidence in the literature that actual structural expansions are (in most cases) much lower than those determined from laboratory prisms. This issue has been partially addressed by Leemann and Merz (2013), Fournier et al. (2009), Lindgård et al. (2010) Lindgård et al. (2012) and Ideker et al. (2012). Furthermore, and despite the (relatively) small size of the walls, material heterogeneity would imply that that one can not *strictu sensus* apply the same AAR property throughout the wall without an attempt to use some homogenization techniques in the spirit of (Xu and Graham-Brady, 2005).

4.3.2 Parameter Identification

Data for expansion over the first 260 days was provided, Table 2 as well as the corresponding degraded tensile strength and elastic modulus, Table 1.

t = 260 days   In Fig. 5 the reported expansions for SW and SW-260 (longitudinal and transverse) in Orbovic et al. (2015) are shown. The indicated points, while not exactly matching the ones in Table 2, they are sufficiently close to be retained.
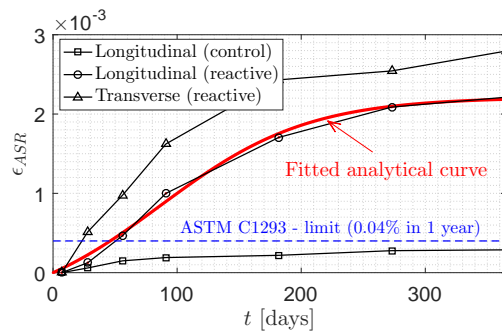
Figure 5: Reported expansion from (Orbovic et al., 2015) and corresponding fitted analytical curve

A simple Matlab code was developed to fit a curve (based on equation 2) to the discrete data points. As a result, the following were obtained: $\tau_c = 81$ days, $\tau_l = 61$ days, and $\varepsilon^\infty = 0.00223$ (0.22%). It should be noted that the concrete expansion at 260 days is relatively small.

t = 1000 days   Determination of the ASR key parameters at 1,000 days is more problematic and values will be extrapolated from the current one with a margin of uncertainty. With reference to Fig. 6(a), expansion up to ~ 250 days is known, and we need to guesstimate the one at time $t = 1,000$ days.

Kinetics: It was assumed that the expansion at that time will obey a uniform distributional model ranging from a minimum 0.25% and a maximum of 0.45%. Then, using a Latin Hypercube sampling (LHS) technique, 100 curves are fitted between those points. The corresponding 100 values of τ_l and τ_c are shown in Fig. 6(b) where the zero values of τ_l are associated with those expansion with a quasi linear early expansion.

(a) Expansion curve

(b) Predicted τ values
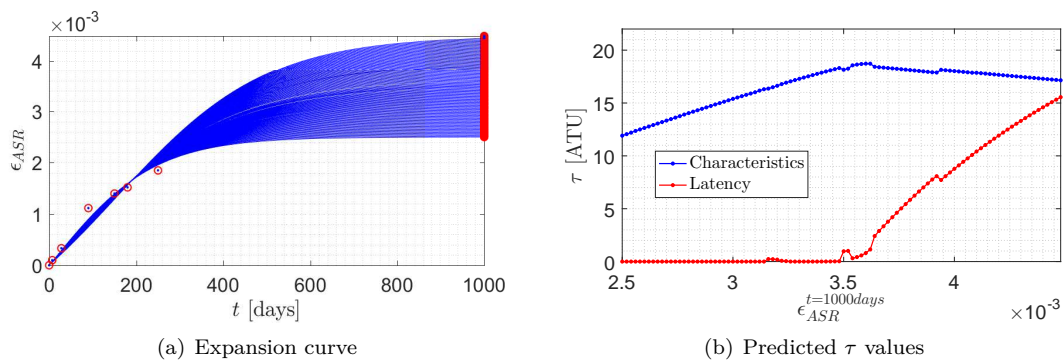
Figure 6: Optimization-based curve fitting to find the future expansion

Deterioration: E and f'_t at time t_0 and t_{260} are given. Using these values a normal distribution model is assumed with the reported values as mean, and a COV reported in Table 4. Then, based on Eq. 4 and the set of 100 values of τ_l and τ_c, degradation curves are obtained, Fig. 7.

(a) f'_t (b) E
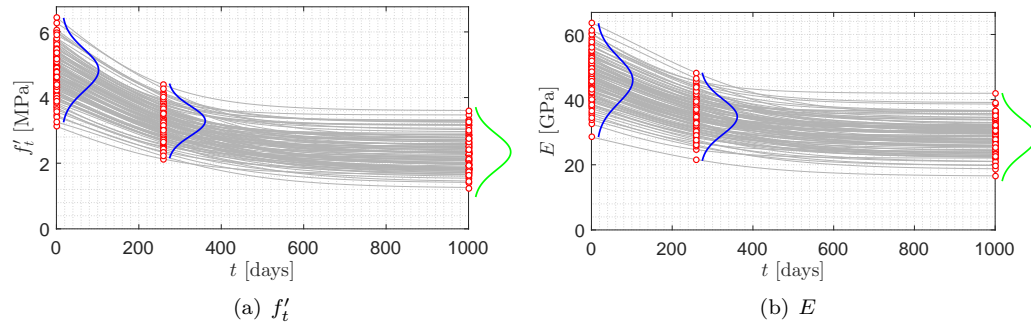
Figure 7: Estimation of residual coefficients

5   Finite Element Model

The prepared finite element mesh is shown in Fig. 8 with consists of quadrilateral elements. There are three layers of elements in the web and five layers in the columns. Top and bottom beams are assumed to be linear elastic while the columns and web have the smeared crack model parameters.

Note that the applied boundary conditions are a reflected idealization of the actual test setup; however, in most such test there is a "slack" with secondary undesirable parasitic displacements which may or may not have contaminated reported values by the experimentalists.

(a) Finite element mesh   (b) Reinforcement   (c) Boundary conditions
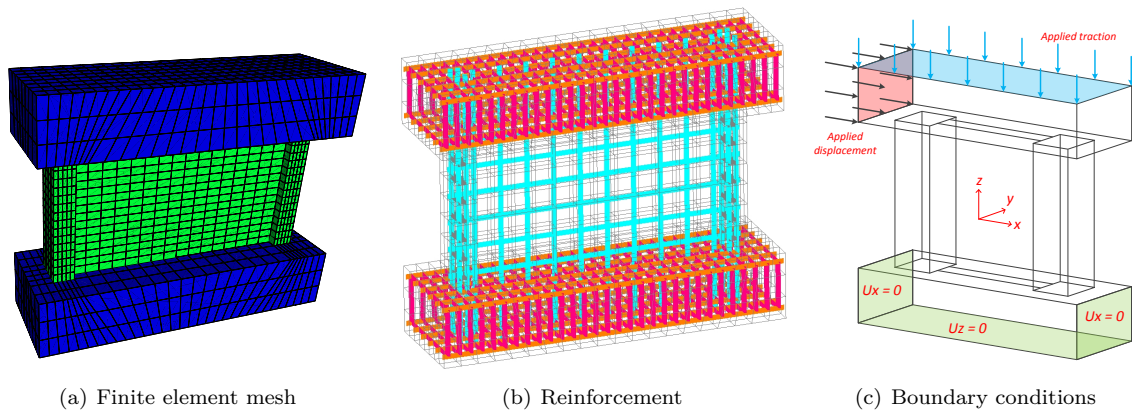
Figure 8: Finite element model

The reported cyclic load is identical to the one shown in Fig. 9(a). However, the figure also shows the 10 intermediary load increment adopted in the analysis. This was achieved through the increments shown in Fig. 9(b).

(a) Cumnulative cyclic displacement

(b) Incremental displacement at each step
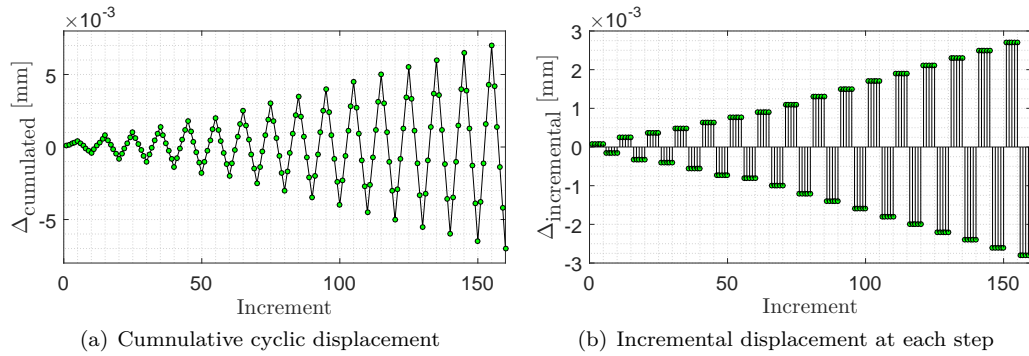
Figure 9: Reversed cyclic loading history applied in numerical analysis

6   Results

Results will be presented as follows:

1. Deterministic analysis of SW and SW-260, followed by calibration.

2. Sensitivity analysis of SW.

3. Uncertainty quantification of SW and SW-1000 along with probability of exceedance of a specific shear wall capacity.

6.1   Deterministic Analysis & Calibration

In this first set of analyses, the meshes shown in Fig. 8 and mean values from Table 4 are used for the SW and SW-260. In the later case, the kinetic curve used is the one shown in Fig. 5. The preliminary envelope for SW is shown in Fig. 10(a). It is evident that the numerical response is too too stiff, and an adjustment has to be made. In light of the experimental uncertainties addressed in sect. 3.1, this discrepancy is attributed to "slack" in the system and an adjustment is to be made. Thus, and in the spirit of this benchmark where calibration is indeed expected first, the displacements are simply multiplied by 2.3. This resulted in a shift of the results which indeed closely match the experimental results. On the other hand, there was no need to adjust forces, as those are not only in good agreement with the experiments but are perceived as more reliable than the experimentally reported displacement. From this point onward, all numerical results will be subjected to this calibration factor.

Then, the results of SW-260 are reported in Fig. 10(b) and again, the two curves are nearly identical.

(a) SW

(b) SW-260
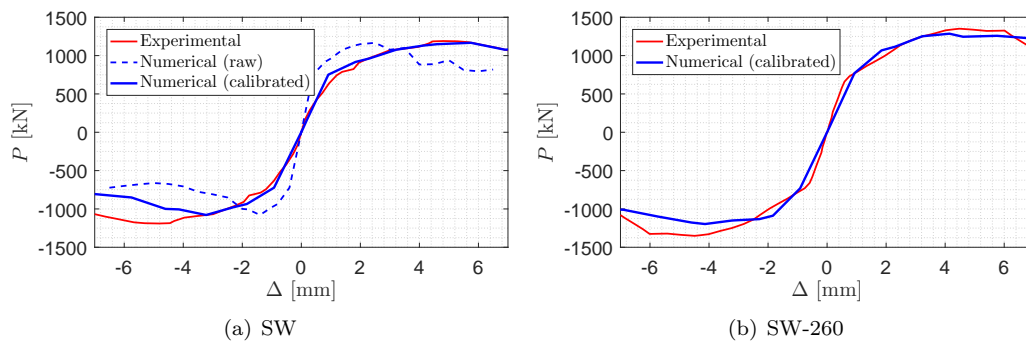
Figure 10: Comparison of the experimental and numerical results at 260 days

For illustrative purpose, the load displacement curve is shown in Fig. 11(a). The deformed shape with maximum principal stresses are shown in Fig. 11(b), and the evolution of the accompanying (smeared)

cracks is finally shown in Fig. 11(c). Visual inspection of these plots provides a graphical confirmation of the reliability of the analysis.

(a) Load-displacement under cyclic load   (b) Deformed shapes; Contour shows the maximum principal strains

(c) Crack propagation in web and columns
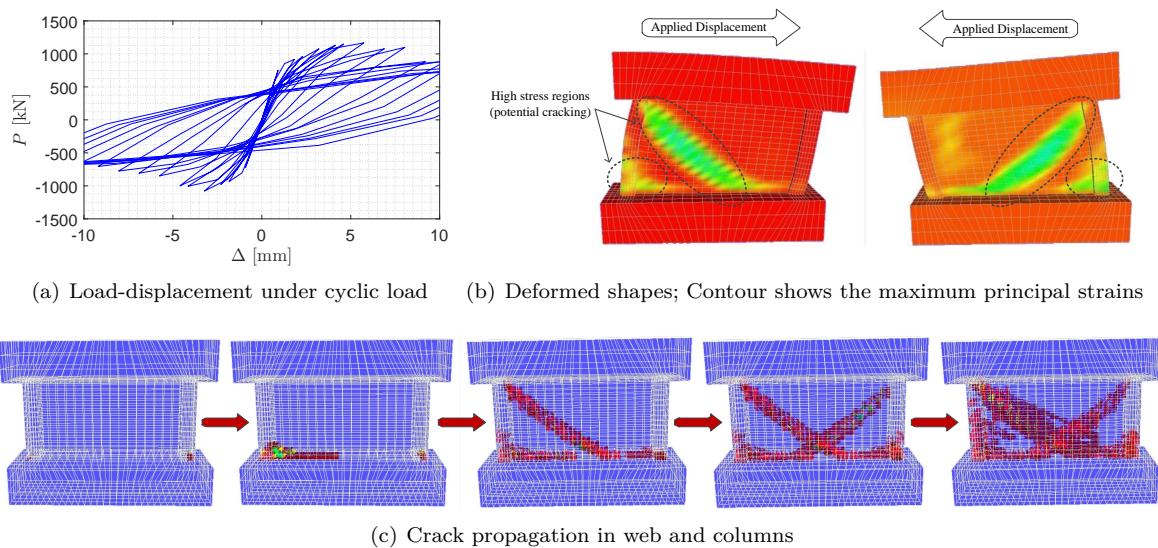
Figure 11: Structural response of shear wall under cyclic displacement (without ASR)

6.2   Sensitivity Analyses

The sensitivity analysis procedure is rooted in the Taylor's Series-Finite Difference Estimation described in Appendix C.

In the context of this analysis, $n = 15$ random variables identified in Table 4 are retained, thus a total of $2n + 1 = 31$ analyses are performed.

First the capacity curves of all the analyses are shown in Fig. 12(a). It is noted that the experimental curve does indeed fall within the range of results, and that in some cases there is an early failure characterized by a sudden drop in the post-peak load carrying curve (whereas some softening resulting from induced displacements would have been expected).

Then the sensitivities are sorted and results shown in the format of a so-called Tornado-Diagram (Lee and Mosalam, 2006). Fig. 12(b).

(a) Capacity curves   (b) Tornado diagram
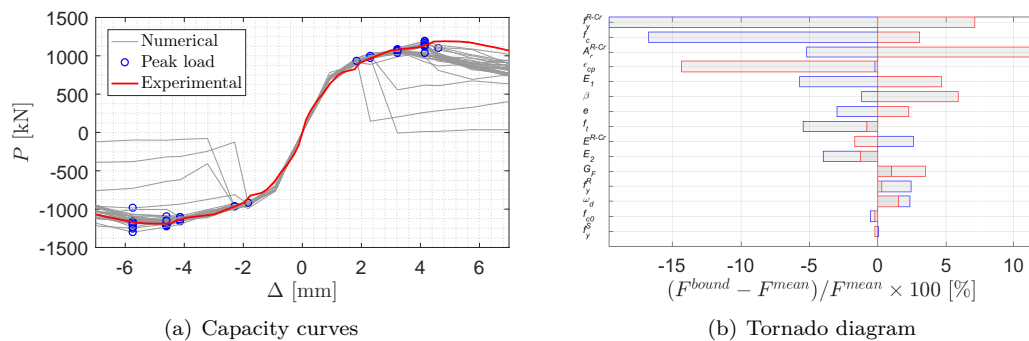
Figure 12: Results of sensitivity analysis on concrete constitutive model

From this figure, it was determined that the steel reinforcement whose crossing the beam-wall interface plays a prominent role in the response through the yield stress and cross-sectional area). As to the concrete,

the predominant variables affecting the shear wall carrying capacity are: the compressive strength, plastic strain at compressive failure, modulus of elasticity are amongst the major factors influencing the response. The least important variables are the yield stress of the stirrups and onset of concrete nonlinearity in compression and concrete compressive critical displacement. Concrete tensile strength and fracture energy are among the intermediary sensitive variables.

It should be emphasized that though the Tornado diagram gives an indication of the response sensitivity to the variables, not all of them are actually random. For instance, the steel properties are well established and as such it need not be treated as a random variable.

6.3   Uncertainty Quantification

Uncertainty quantification has retained the variables listed in Table 4 as random with a normal PDF. Selection of those are based on the Tornado diagram and engineering common sense.

6.3.1   Automation of Probabilistic Analysis

Given the complexity in data manipulation from input data definition, random variable selection, generation of finite element meshes, execution, data mining to extract results, and plotting key diagrams an automated procedure was set up. This was accomplished through a Matlab based set of sequential programs `P1.m`, `P2.m, P3.m, P4.m` and `P5.m` whose inter-connectivity is illustrated in Fig. 13.
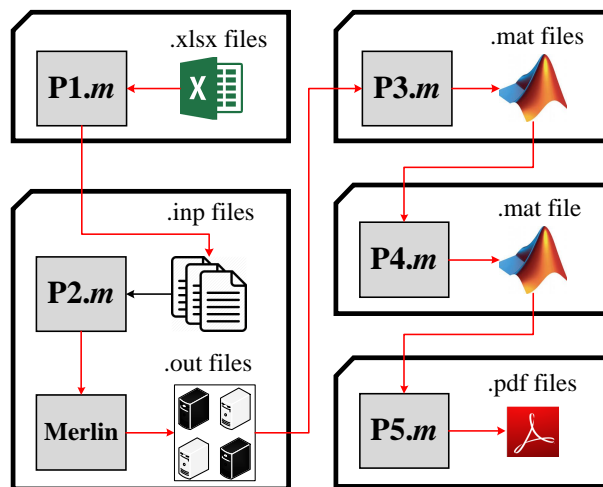
Figure 13: File generation and automation algorithm

`p1.m` reads the user specified variables, probability distribution models, ranges, and correlation coefficients, and then generates the 121 input files. Those in turn are executed through `p2.m` which calls the finite element code Merlin. On average, each analysis required results are then individually extracted from 121 output files and stored as binary files (`p3.m`) and consolidated into a single data-base (`p4.m`). Finally, `p5.m` extract the results from the data base and generates the desired results. For each output parameter, results are plotted along with their mean, 16 and 84 fractiles ranges (which correspond to minus and plus one standard deviation in a log-normal distributional model).

6.3.2   Prediction

Following completion of the 100 analyses (it should be noted that five analyses did not converge most likely due to an unfavourable set of ASR material parameters), `P5.m` generated the capacity curves for SW and SW-1000, Fig. 14. Then, the 16% and 84% fractile curves are sought. This is simply achieved by sweeping through the full range of displacements, and for each one identify the points below which 16% and 84% of

the load fall. These correspond to mean plus or minus one standard deviation in a normal distribution Fig. 4.

As with Fig. 12(a) the capacity curves for SW, Fig. 14(a) is in close agreement with the experimental data. However, contrarily to the first sensitivity analysis, the uncertainty one shows that the experimental tests fall within the 16th and 84th fractile.

Finally, we reach the objective of this investigation which is to provide a probabilisitc based assessment of the shear wall capacity when tested 1,000 days after casting. This is shown in Fig. 14(b). It is worthy to note how tight the 16% and 84% curves are with respect to the mean. It is the expectation of this study that, assuming that the experiments were perfectly performed, data properly recorded, the experimental curve would be within those two curves.
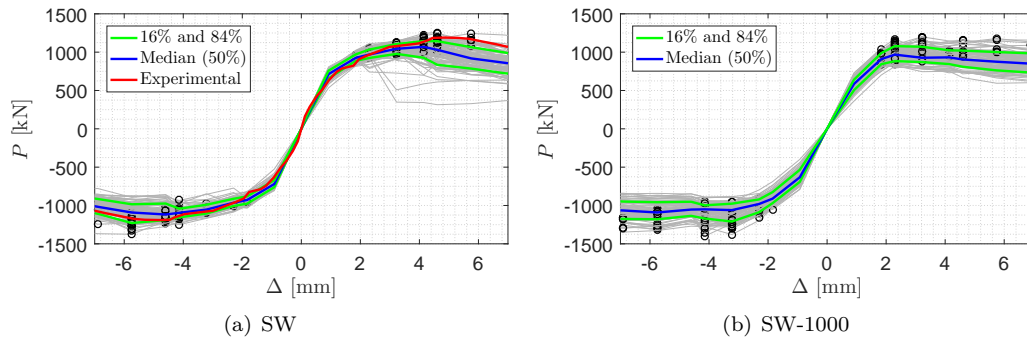
Figure 14: Results of uncertainty quantification on capacity curves

Results warrant additional examination to fully grasp the structural responses. As such, Figure 15(a) plots the shear wall capacity for SW and SW-1000 along with the corresponding histograms and fitted lognormal distribution function. Fig. 15(b) shows the cumulative distribution functions for empirical (dashed lines) and fitted (continuous lines) for both SW and SW-1000. Mean and logarithmic standard deviation are 1.14 MN and 0.090 MN for SW, and 1.13 MN and 0.11 MN for SW-1000 respectively. It should be noted that there is wider SD in SW-1000 as there are more RV's.

It should also be noted that in $\sim 60\%$ of the analysis the shear capacity was reduced by the pre-existence of ASR, and in $\sim 40\%$ it increased.

This is caused by prepare an excel file, 100 rows, 11 columns, and add P˙max^SW P˙max^SW-1000, then we can sort based on the ratios of P˙max
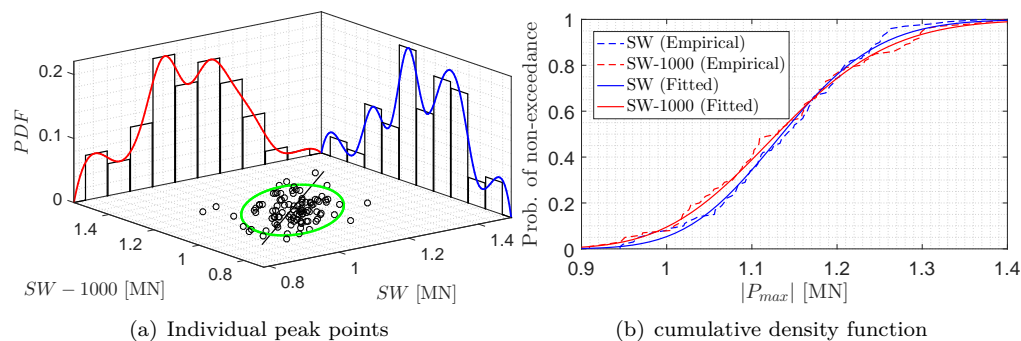
Figure 15: Comparison of SW and SW-1000 models

Finally, a similar scheme where ASR may increase or reduce the shear strength capacity was observed by the authors in a separate study, (Saouma et al., 2016) shown in Fig. 16. The monotonic shear strength of a panel was numerically determined with and without initial AAR expansion. In both cases, the initial stiffness was reduced by ASR. Regretfully, it was not possible to clearly identify the set of parameters which cause

(a) Shear capacity reduction   (b) Shear capacity increase
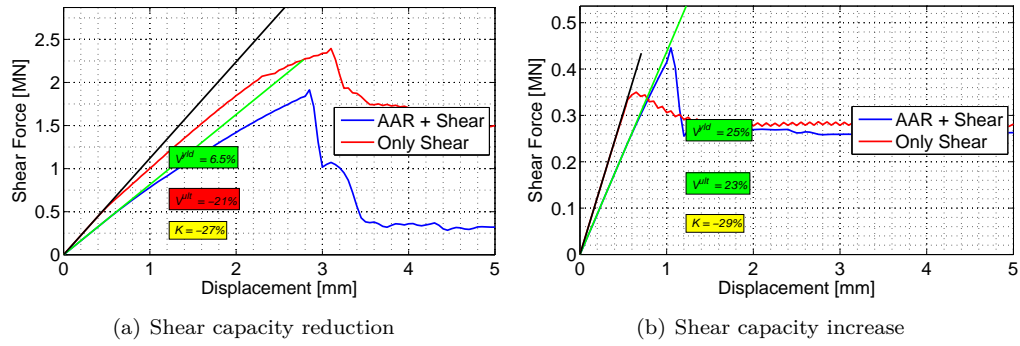
Figure 16: Impact of ASR on shear capacity of concrete panels from a NPP (Saouma et al., 2016)

an increase (or decrease) in shear strength capacity due to previous AAR. This remains an open question of the utmost importance which requires further in depth study.

7   Conclusions

Rather than focusing on the numerical evaluation of the shear wall strength after having undergone a thousand days of AAR caused expansion, a different approach was taken. It was recognized that there are too many experimental and epistemic uncertainties, and as such a Monte-Carlo based uncertainty quantification was performed. This was preceded by a sensitivity analysis to assess those model variables most likely to impact the results.

Results are then presented in a probabilistic context.

Finally, the study highlighted the fact in some cases AAR increased the shear wall capacity, while in other it decreased it. This is a topic that warrants further investigation as it may have abig impact on the assessment of shear critical structures suffering from AAR.

8   Acknowledgments

References

ADAMS Accession No. ML 121160422 (2012). *Impact of Alkali Silica Reaction on Seabrook Concrete Structure*. Tech. rep. NextEra.

Amberg, F. (2011). "Performance of dams affected by expanding concrete". In: *Dams and Reservoirs under Changing Challenges*, p. 115.

Army Corps of Engineers (1992). *Reliability Assessment of Navigation Structures*. ETL 1110-2-532. Washington, D.C.: Department of the Army, US Army Corps of Engineers.

— (1993). *Reliability Assessment of Navigation Structures; Stability of Existing Gravity Structures*. ETL 1110-2-321. Washington, D.C.: Department of the Army, US Army Corps of Engineers.

Ben-Ftima, M., H. Sadouki, and E. Bruhwiler (2016). "Development of a computational multi-physical framework for the use of nonlinear explicit approach in the assessment of concrete structures affected by alklai-aggregate reaction". In: *9th International Conference on Fracture Mechanics of Concrete and Concrete Structures; FraMCoS-9*. Ed. by V.E. Saouma, J. Bolander, and E. Landis. Berkeley, CA. URL: \url{http://dx.doi.org/10.21012/FC9.221}.

Benjamin, J. and C.A. Cornell (1970). *Probability, Statistics, and Decision for Civil Engineers*. New York: McGraw Hill.

Bryant, L.M., J.T. Brokaw, and P.F. Mlakar (1993). *Reliability Modeling of Concrete Overstressing*. Tech. rep. Report Submitted to U.S. Army Engineer Waterways Experiment Station. JAYCOR, Vicksburg Mississippi.

Capra, B. and J.P. Bournazel (1998). "Modeling of induced mechanical effects of alkali-aggregate reactions". In: *Cement and Concrete Research* 28.2, pp. 251–260.

Cervenka, J. and V.K. Papanikolaou (2008). "Three Dimensional Combined Fracture-Plastic Material Model for Concrete". In: *International Journal of Plasticity* 24.12, pp. 2192–2220.

Der Kiureghian, A. and O. Ditlevsen (2009). "Aleatory or epistemic? Does it matter?" In: *Structural Safety*, pp. 105–112.

El Mohandes, F. and F.J. Vecchio (2013). *VecTor3: A. User's Manual; B. Sample Coupled Thermal and Structural Analysis*. Dept. of Civil Engineering, University of Toronto. Toronto, Canada.

Fournier, B. et al. (2009). "Effect of environmental conditions on expansion in concrete due to alkali–silica reaction (ASR)". In: *Materials Characterization* 60.7, pp. 669–679.

Habibi, F. et al. (2015). "Alkali Aggregate Reaction In Nuclear Concrete Structures: Part 3: Structural Shear Wall Elements". In: *Proceedings of the 23rd Conference on Structural Mechanics in Reactor Technology (SMiRT23)*.

Hariri-Ardebili, M., V.E. Saouma, and Y. LePape (2016). *Independent Modeling of the Alkali-SilicaReaction: Mock-up Test Block*. Tech. rep. ORNL/TM-2016/537. Oak Ridge, TN 37831: Oak Ridge National Laboratory.

Hariri-Ardebili, M.A. and V. Saouma (2016a). "Probabilistic seismic demand model and optimal intensity measure for concrete dams". In: *Structural Safety* 59, pp. 67–85.

Hariri-Ardebili, M.A. and V.E. Saouma (2016b). "Sensitivity and Uncertainty Quantification of the Cohesive Crack Model". In: *Engineering Fracture Mechanics* 155, pp. 18–35.

Huang, H. and B. Spencer (2016). "Grizzly model for fully coupled heat transfer, moisture, diffusion, alkali-silica reaction and fractureing process in concrete". In: *9th International Conference on Fracture Mechanics of Concrete and Concrete Structures; FraMCoS-9*. Ed. by V.E. Saouma, J. Bolander, and E. Landis. Berkeley, CA. URL: \url{http://dx.doi.org/10.21012/FC9.194}.

Huang, H., B. Spencer, and G. Cai (2015). *Grizzly Model of Multi-Species Reactive Diffusion, Moisture/Heat Transfer, and Alkali-Silica Reaction in Concrete*. Tech. rep. INL/EXT-15-36425. Idaho Falls, Idaho 83415: Idaho National Laboratory.

ICOLD Bulletin 79 (1991). *Alkali-Aggregate Reaction in Concrete Dams*. Tech. rep. International Commission on Large Dams.

Ideker, J.H. et al. (2012). "Do current laboratory test methods accurately predict alkali-silica reactivity?" In: *ACI Materials Journal* 109.4.

Le Pape, Y. and Ma, Z. and Cabage, J. and Lenarduzzi, R. (2014). *Design of a large-scale concrete mockup to study the effects of alkali-silica reaction on expansion, damage and shear fracture propagation in stress-confined safety related structures*. Tech. rep. Technical Report M3LW-14OR-0403012 - Rev. 1. Light Water Reactor Sustainability Program.

Lee, T.H. and K.M. Mosalam (2006). *Probabilistic seismic evaluation of reinforced concrete structural components and systems*. Tech. rep. 2006/04. Pacific Earthquake Engineering Research Center.

Leemann, Andreas and Christine Merz (2013). "An attempt to validate the ultra-accelerated microbar and the concrete performance test with the degree of AAR-induced damage observed in concrete structures". In: *Cement and Concrete Research* 49, pp. 29–37.

Lindgård, Jan et al. (2010). "The EU "PARTNER" Project-European standard tests to prevent alkali reactions in aggregates: final results and recommendations". In: *Cement and Concrete Research* 40.4, pp. 611–635.

Lindgård, Jan et al. (2012). "Alkali–silica reactions (ASR): literature review on parameters influencing laboratory performance testing". In: *Cement and Concrete Research* 42.2, pp. 223–243.

Marquié, C. (2016). *IRSN R&D on Concrete Pathologies Issues: The ODOBA Project*. URL: \url{https://www.nrc.gov/public-involve/conference-symposia/ric/past/2016/docs/abstracts/marquiec-t7-hv.pdf}.

Mirzabozorg, H. (2013). Personal Communication.

Murazumi, Y. et al. (2005a). "Study of the influence of alkali-silica reaction on mechanical properties of reinforced concrete members". In: *18th International Conference on Structural Mechanics in Reactor Technology (SMIRT 18)*. SMIRT18-H03-3. Beijing, China, pp. 2043–2048.

Murazumi, Y. et al. (2005b). "Study of the influence of Alkali-Silica Reaction on structural behavior of reinforced concrete members". In: *18th International Conference on Structural Mechanics in Reactor Technology (SMIRT 18)*. SMIRT18-H03-2. Beijing, China, pp. 2036–2042.

Naus, D. (2007). *Primer on Durability of Nuclear Power Plant Reinforced Concrete Structures - A Review of Pertinent Factors*. Tech. rep. NUREG/CR-6927 ORNL/TM-2006/529. U.S. Nuclear Regulatory Commission.

NRC-CU Grant (2014). *Experimental and Numerical Investigation of Alkali Silica Reaction in Nuclear Reactors*. Tech. rep. Grant and Cooperative Agreement NRC-HQ-60-14-G-0010. URL: \url{https://www.nrc.gov/docs/ML1427/ML14274A265.pdf}.

NRC-NIST Project (2014). *Structural Performance of Nuclear Power Plant (NPP) Concrete Structures Affected by Alkali-Silica Reaction (ASR)*. Tech. rep. Interagency Agreement No. NRC-HQ-60-14-I-0004. URL: \url{https://www.nrc.gov/docs/ML1414/ML14147A221.pdf}.

Orbovic, N. (2011). *Personal Communication*. Canadian Nuclear Safety Commission.

Orbovic, N. et al. (2015). "Alkali Aggregate Reaction in Nuclear Concrete Structures: Part 1: A Holistic Approach". In: *Proceedings of the 23rd Conference on Structural Mechanics in Reactor Technology (SMiRT23).*

Pan, J. et al. (2013). "Numerical prediction of swelling in concrete arch dams affected by alkaliaggregate reaction". In: *European Journal of Environmental and Civil Engineering* 17.4, pp. 231–247.

Pian, J.W. et al. (2012). "Modeling of alkali-silica reaction in concrete: a review". In: *Front. Struct. Civ. Eng.* 6.1, pp. 1–18. DOI: {10.1007/s11709-012-0141-2}.

Rodriguez, J. et al. (2011). "Contribution to Theme A of the Benchmark Workshop: Effect of Concrete Swelling on the Equilibrium and Displacements of an Arch Dam". In: *Proceedings of the XI ICOLD Benchmark Workshop on Numerical Analysis of Dams.* Valencia, Spain.

Saouma, V. (2005). "Reliability Based Nonlinear Fracture Mechanics Analysis of a Dam". In: *Dam Engineering* 16.3, pp. 219–241.

— (2013a). "Applications of the cohesive crack model to concrete, ceramics and polymers". In: *Proceedigs of the 8th International Conference on the Fracture Mechanics of Concrete and Structures.* Invited Pleanry Lecture. Toledo, Spain.

Saouma, V.E. (2013b). *Numerical Modeling of Alkali Aggregate Reaction.* 320 pages. CRC Press.

Saouma, V.E., M. Hariri-Ardebili, and Y. Le Pape (2015). *Effect of Alkali-Silica Reaction on Shear Strength of Reinforced Concrete Structural Members.* Tech. rep. ORNL/TM-2015/588. Oak Ridge, TN 37831: Oak Ridge National Laboratory.

Saouma, V.E. and L. Perotti (2006). "Constitutive Model for Alkali Aggregate Reactions". In: *ACI Materials Journal* 103.3, pp. 194–202.

Saouma, V.E., J. Červenka, and R. Reich (2010). *Merlin Finite Element User's Manual.* URL: \url{http://civil.colorado.edu/~saouma/pdf/users.pdf}.

Saouma, V.E. et al. (2015). "A Mathematical Model for the Kinetics of the Alkali-Silica Chemical Reaction". In: *Cement and Concrete Research* 68, pp. 184–195.

Saouma, V.E et al. (2016). "Effect of alkali–silica reaction on the shear strength of reinforced concrete structural members. A numerical and statistical study". In: *Nuclear Engineering and Design* 310, pp. 295–310.

Saouma, V.E. et al. (2017). *Benchmark Problems for AAR FEA Code Validation.* URL: \url{http://www.rilem.org/global/gene/doc_link.php?doc=2016161048_rilem-tc-259-isr-wg2-benchmark.pdf}.

Saouma, V.E. and Hariri-Ardebili, M. and Puatsananon, W. and Le Pape, Y. (2014). *Preliminary Results on the Structural Significance of Alkali-Silica Reaction in Massive Reinforced Concrete Structures.* Tech. rep. ORNL/TM-2014/489. Oak Ridge, TN 37831: Oak Ridge National Laboratory.

Sheikh, S. (20017). Personal Communication, March 10, 2017.

Shimizu, H. et al. (2005a). "Investigaiton of Safety Margin for Turbine Generator Foundation Affected by Alkali-Silica Reaction Based on Non-Linear Structural Analysis". In: *18th International Conference on Structural Mechanics in Reactor Technology (SMIRT 18).* SMIRT18-H03-4. Beijing, China, pp. 2049–2059.

Shimizu, H. et al. (2005b). "Study on Material Properties in Order to Apply for Structural Analysis of Turbine Generator Foundation Affected by Alkali-Silica Reaction". In: *18th International Conference on Structural Mechanics in Reactor Technology (SMIRT 18).* SMIRT18-H03-5. Beijing, China, pp. 2055–2060.

Takagkura, T. et al. (2005). "Structural soundness for turbine-generator foundation affected by alkali-silica reaction and its maintenance plans". In: *18th International Conference on Structural Mechanics in Reactor Technology (SMIRT 18).* SMIRT18-H03-5. Beijing, China, pp. 2055–2060.

Takatura, T. et al. (2005a). "Investigation of the expanded value of turbine generator foundation affected by alkali-silica reaction". In: *18th International Conference on Structural Mechanics in Reactor Technology (SMIRT 18).* SMIRT18-H03-7. Beijing, China, pp. 2061–2068.

Takatura, T. et al. (2005b). "Vibration measurement and simulation analysis on a reinforced concrete structure with alkali-silica reaction". In: *18th International Conference on Structural Mechanics in Reactor Technology (SMIRT 18).* SMIRT18-H03-1. Beijing, China, pp. 2026–2035.

Tcherner, J. and T. Aziz (2009). "Effects of AAR on Seismic Assessment of Nuclear Power Plants for Life Extensions". In: *20th International Conference on Structural Mechanics in Reactor Technology (SMIRT 20).* SMIRT20-Division 7 Paper 1789. Espoo, Finland.

Thacker, B.H. et al. (2004). *Concepts of Model Verification and Validation*. Tech. rep. LA-14167. Los Alamos National Laboratory. URL: \url{http://www.osti.gov/scitech/biblio/835920-Yl8Ow3/native/}.

Xu, X. and L. Graham-Brady (2005). "A stochastic computational method for evaluation of global and local behavior of random elastic media". In: *Computer methods in applied mechanics and engineering* 194.42, pp. 4362–4385.

A   Communication with U. Ottawa

VS: Victor Saouma; **NO:** Nebojsa Orbović; **SS:** Shamim Sheikh (U. of Ottawa).

VES: Can you please (urgently?) send us information on how are the lateral displacements measured in the tests?

NO: The lateral displacements are not measured they were imposed.

VES: Thanks, and I would like to see a picture of the locations of the LVDT and their measurements. From my (dare I say extensive) experience, no matter how much you may have tightened/bolted the wall, there will always be some slack/slip, which is why we measure it separately.

VES: Well I a would like to know if they measured the slack, I.e some rigid body motion which always occur in such tests and which should be subtracted from the imposed displacement.

SS: The displacement provided is what is measured between the bottom of the upper beam and the top of the lower beam. A picture (Fig. 17) and a sketch are provided to show this. The actuator displacements are not provided.
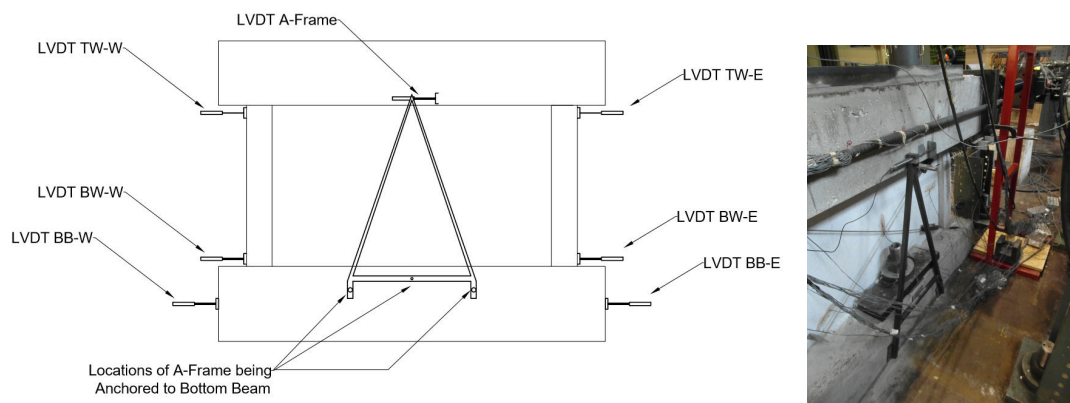
Figure 17: Clarifications regarding displacement measurements (Sheikh, 20017)

VES: Thanks much better but the displacement imposed by the actuator (since you are in stroke and not strain control) is obviously not the same as the one recorded by the lvdt. May I please ask you to clarify:

1. you are programming your setup in stroke (actuator) or strain (if so which lvdt) controls?
2. your load-displacement curve that you report, displacement is from which lvdt?

SS: I will give you my recollection of what my student and I discussed long time ago. I will not bother my student at 9.30 pm on Friday. We ran the test "almost manually". The load was applied by controlling actuator's LVDT stroke but the feed was from the LVDTs recording the displacement of the top of the lower beam and the bottom of the upper beam. The displacement shown on the graphs was determined after carefully comparing all the combinations of LVDT measurements including the

bottom beam LVDTs. Due to slight differences in locations of LVDTs, some geometric corrections had to be made. We believe that the graph given is the true reflection of the measured response of the wall panel between the beams.

VES: Hum, my apologies for persisting in seeking the clearest clarifications:

1. You had two actuators, one on each side. Were they both capable of push and pull, or simply push (i.e. push from the left, relax, push (back) from the right one). In other word, all the positive slope in the displacement vs time were with one actuator, and the negative one with the other. Correct?

2. The test was run in displacement control and not load control. That is you imposed a displacement. I you wanted to impose a total displacement of 3 mm from current position, then you manually turned the knob until the actuator lvdt recorded 3mm. Correct?

3. But then, if you move back and forth with actuator, when you switch you need to unload, record the inelastic deformation, and then apply a a commensurate displacement from the other one. Correct?

4. Finally, for the plotted hysteretic reported load displacement, you used the actuator load cell and some sort of average/corrected LVDT readings. Presumably those two reading were synched in your data acquisition system. Correct?

5. Same procedure was used in al four batch of tests (early late tests, reactive, non reactive)?

Again, I am sorry to be that pick, but it is important for me to understand the subtelity of this complex test before I run any finite element analysis.

SS: Here are our answers to your questions:

1. Up to 1000 kN one actuator pushes only and the other one just follows the displacement freely. Once the pushing actuator limit of 1000 kN is achieved, the other one gets engaged and pulls as well.

2. Test was done in displacement control. The imposed displacement was controlled using both A-Frame and the difference between the values obtained from the LVDTs at top of the wall and the bottom of the wall from both sides.

3. At the end of a cycle, the actuators were kept in place, and opposite loading protocol was applied. Next the actuator previously pushing will be pulling, and the one that was pulling will push. Throughout each cycle the displacement rate was kept constant.

4. Your descrition is correct.

5. Your descrition is correct again.

B   AAR Constitutive Model

The theoretical underpinning of the AAR model used in this paper has been presented by the authors separately, Saouma and Perotti, 2006 and Saouma, 2013b. It will be briefly reviewed.

The AAR expansion is considered to be a volumetric one, which rate is given by the following function

$$\dot{\varepsilon}_V^{AAR}(t, \theta, RH) = \Gamma_t(f_t'|w_c, \sigma_I|COD_{max}) \, \Gamma_c(\overline{\sigma}, f_c') \\ g(RH) \, \dot{\xi}(t, \theta) \, \left. \varepsilon^\infty \right|_{\theta=\theta_0} \tag{1}$$

where ε^∞ is the final volumetric expansion as determined from laboratory tests at temperature θ_0. $0 \leq \Gamma_t \leq 1$ is a parameter which reduces the expansion in the presence of large tensile stresses (macro-cracks absorbing the gel), f_t' the tensile strength, and σ_I the major (tensile) principal stress. Similarly, $0 \leq \Gamma_c \leq 1$ is a parameter which accounts for the absorption of the gel due to compressive induced stresses, $\overline{\sigma}$ and f_c' are the

hydrostatic stress, and the compressive strength of the concrete, respectively. $0 \leq g(RH) \leq 1$ is a function of the relative humidity (set to zero if the humidity is below 80%), $\dot{\xi}(t,\theta)$ the kinetics law given by

$$\xi(t,\theta) = \frac{1 - \exp(-\frac{t}{\tau_c(\theta)})}{1 + \exp\left(-\frac{(t-\tau_l(\theta))}{\tau_c(\theta)}\right)} \tag{2}$$

where τ_l and τ_c are the latency and characteristic times, respectively. The former corresponds to the inflexion point, and the latter is defined in terms of the intersection of the tangent at τ_l with the asymptotic unit value of ξ, figure 18(a). They are given by

$$\begin{aligned}
\tau_l(\theta) &= \tau_l(\theta_0)\exp\left[U_l\left(\frac{1}{\theta} - \frac{1}{\theta_0}\right)\right] \\
\tau_c(\theta) &= \tau_c(\theta_0)\exp\left[U_c\left(\frac{1}{\theta} - \frac{1}{\theta_0}\right)\right]
\end{aligned} \tag{3}$$

expressed in terms of the absolute temperature ($\theta^o K = 273 + T^o C$) and the corresponding activation energies. U_l and U_c are the activation energies, minimum energy required to trigger the reaction for the latency and characteristic times, respectively. Once the volumetric AAR strain is determined, it is decomposed into a tensorial strain in accordance to the three weight factors associated with the principal stresses. Finally, degradation of the tensile strength and elastic modulus is accounted for as follows:

$$\begin{aligned}
E(t,\theta) &= E_0\left[1 - (1 - \beta_E)\,\xi(t,\theta)\right] \\
f_t(t,\theta) &= f_{t,0}\left[1 - (1 - \beta_E)\,\xi(t,\theta)\right]
\end{aligned} \tag{4}$$

The model is relatively simple to implement in an existing finite element code and has been implemented in many finite element codes Pian et al., 2012 El Mohandes and Vecchio, 2013, Rodriguez et al., 2011 Mirzabozorg, 2013 Pan et al., 2013 Huang and Spencer, 2016 Huang, Spencer, and Cai, 2015 Ben-Ftima, Sadouki, and Bruhwiler, 2016.

In the context of this study, there are no good estimate for: 1) what would be the ultimate AAR induced strain as possibly determined from reliable laboratory residual expansion (not a simple task); and 2) what is the internal relative humidity in the box girder ($g(RH)$ in Eq. 1). Indeed, it has long been recognized that for AAR to occur, RH must be above a certain threshold Capra and Bournazel, 1998.

The effect of temperature and relative humidity on the kinetics of the reaction is illustrated by figure 18(a) where the decrease in RH, results in a decrease of peak AAR while a in temperature will slow the reaction. Finally, The engineering significance of the (sigmoid) expansion is illustrated in figure 18(b) Saouma et al., 2015.

(a) Effect of temperature and relative humidity   (b) Physical interpretation
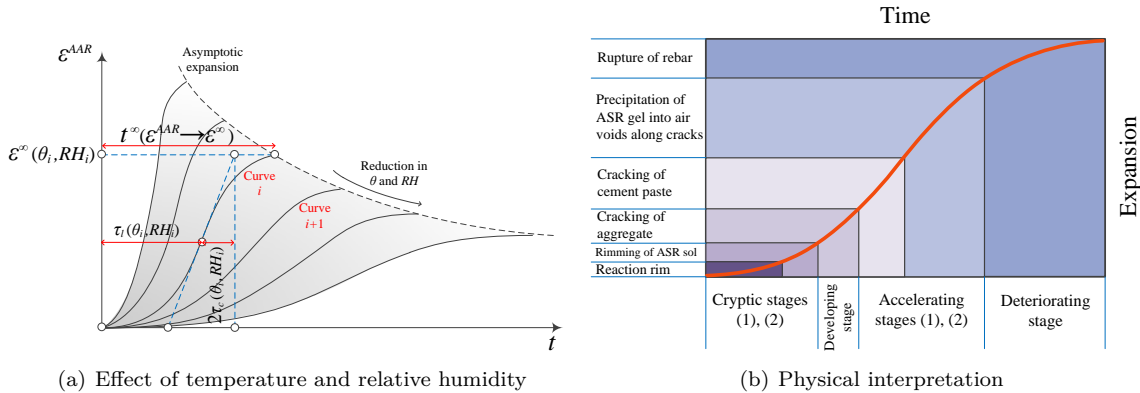
Figure 18: AAR expansion curve Saouma et al., 2015

C   Taylor's Series-Finite Difference Estimation

The concept behind the sensitivity analysis is rooted in the so-called Taylor's series finite difference estimation of the mean μ in terms of all the random variables individual means μ_i is the mean for all random variables Bryant, Brokaw, and Mlakar, 1993. Hence, for an independent random variables, the variance is given by

$$\mu_F = F(\mu_i) \tag{5}$$

where

$$Var(F) = \sigma_F^2 \quad = \quad \sum \left(\frac{\partial F}{\partial x_i} \sigma_i \right)^2 \tag{6}$$

$$\frac{\partial F}{\partial x_i} \quad \approx \quad \frac{F_i^+ - F_i^-}{2\sigma_i} \tag{7}$$

$$F_i^+ \quad = \quad F(\mu_1, \cdots, \mu_i + \sigma_i, \cdots, \mu_n) \tag{8}$$

$$F_i^- \quad = \quad F(\mu_1, \cdots, \mu_i - \sigma_i, \cdots, \mu_n) \tag{9}$$

where σ_i are the standard deviations of the variables. Hence,

$$\sigma_F = \sum \left(\frac{F_i^+ - F_i^-}{2} \right) \tag{10}$$

The procedure can be summarized as follows:

1. Perform an initial analysis in which all variables are set equal to their mean value. This analysis provides the mean μ.

2. Perform $2n$ analysis, in which all variables are set equal to their mean values, except variable i, which assumes a value equal to $\mu_i + \sigma_i$, and then $\mu_i - \sigma_i$.

3. For each pair of analysis in which variable x_i is modified, determine the standard deviation component associated with the specific variable i, which will provide an indication of the *sensitivity* of the results to variation of this particular variable. $\left(\frac{F_i^+ - F_i^-}{2} \right)$.

4. The standard deviation of the entire structure is then determined by simply adding all the $\left(\frac{F_i^+ - F_i^-}{2} \right)$ terms.

5. Sort the results in an descending order and form the so-called "Tornado diagram".

This simplified method has been first reported by Benjamin and Cornell (1970) in the context of structural engineering, and then used in (Army Corps of Engineers, 1992) (Army Corps of Engineers, 1993) and (Saouma, 2005).

D   Tabulation of Submitted Results

In order to compare/contrast this presentation with the one of other participants, we have summarized the results submitted in Table 5

E   Critical Assessment of the 2017 ASCET Benchmark

As expressed in our submission, presentation and during the workshop, Colorado has serious reservation about hasty conclusions that may be drawn from the presented results.

Having said that, this was a fruitful exercise as it highlighted some of the complexities in finite element modeling in general and AAR in particular.

A-priori, we were asked to model a seemingly simple test. Yet:

Table 5: Summary of ASCET 2017 submitted results

No	Team	Author	Model type	Software	Concrete model	Steel type	ASR model	Top and bottom beam	Cyclic load type	BC	analysis type	Results at 260 days	Results at 1000 days	Explanation
1	Cachan	Kishta, Benboudjema, Nahas	2D + 3D	Cast3M	Damage model of Mazars with an energy-based regularization	1D linear elastic bar element	Poyet (2003). It is based on thermal expansion (isotropic swelling by temperature)	linear elastic	-	-	Deterministic	L-D curves are about the same. No crack pattern is shown.	No	1) impact of reinforcement is studied. 2) the accounted for the random swelling effect.
2	CNSC-Canada	Sagals	2D shell model	LS_Dyna (explicit solution)	concrete cracking and crushing	smeared with yielding	equivalent thermal expansion. No real ASR model is used.	-	applied on two sides with rigid plates	bottom beam is fixed in vertical direction in its upper face	Deterministic	Capacity of regular concrete is close to test but they overstimated ASR affected concrete. L D curves have lots of noise.	predicted ASR expansion in 1000 days is identical to 260 days.	1) cyclic load is applied in quasi-static form. 2) 2D shell mesh calibrated with 3D solid mesh. 3) mesh density tested. 4) limited sensitivity analysis on impact of expansion and concrete compressive strength.
3	Colorado	Saouma, Hariri-Ardebili	3D	Merlin-Matlab	Fracture mechanics based smeared crack	smeared elasto perfectly plastic	Saouma model	linear elastic	applied on one side of top beam	bottom beam is fixed at sides	probabilistic	Deterministic calibration of results matches well for both regular and ASR affected models. For probabilistic one, the test falls in the mean +- std of results	There is 60% chance that the shear capacity decreases and 40% chance of increasing. Crack pattern follows both the diagonal and horizontal base cracks.	1) a fully automated program is developed. 2) Full Sensitivity analysis followed by tornado diagram is provided. 3) Uncertainty quantification is performed in 260 and 1000 days with 121 analysis for each. 4) material randomness is taken into account. 5) Future temporal uncertainty in ASR expansion is taken into account by uniform Latin hypercube sampling. 6) time-dependent material degradation is taken into account.
4	EdF	Etienne, Damien, Etienne, Pierre, Sylvere	3D (one-half of the wall)	Aster	anisotropic plastic	1D element with plastic behaviour	Sellier	top beam can rotate.	Concentrated load is applied on side of the beam.	bottom of the lower beam is subjected to unilateral contact (free to move up). System is only connected to "earth" by a center screw.	Deterministic	The major crack opening starts in diagonal form not at the base of columns. There is only one major diagonal crack (not two crossing).	ASR affected model has higher capacity than regular wall. Also, 260 and 930 days models are nearly identical.	1) Creep model is included.
5	Ferche and Vecchio	Ferche, Vecchio	2D plane stress	VecTor2	Smeared rotating crack model	Smeared reinforcement (ductile and structural)	Not Clear	-	concentrated displ is applied at mid-depth of top beam in middle	constrained only on the bottom of lower beam. No crack pattern is shown.	Deterministic	for regular concrete they overstimated experiment but for ASR affected one it is about the same.	they overstimated the experiment for both regular and ASR affected.	1) both monotonic and cyclic displacements are applied. 2) single 2D model is calibrated by 3D model
6	Kansai	Ueda, Nakamura	3D	?	Lattice equivalent continuum model (fixed crack model)	bilinear truss element	Ref [1] ?	-	concentrated displ is applied at mid-depth of top beam on both sides.	bottom beam is fixed at bottom and sides.	Deterministic	no meaningfull difference	no meaningfull difference. No crack pattern is shown	1) the bond interaction between concrete and reinforcement is taken into account. 2) E, ft and fc are reduced with increase of the expansive strain though an empirical equation. 3) they considered two senario for expansion: optimism (nearly no change after 260 days), pessimism (twice the expansion)
7	Nagoya	Yamamoto, Miura, Nakamura	3D (rigid-body-spring model)	?	consist of normal and shear springs	beam element with zero size link element	not clear (Sellier)	-	concentrated displ is applied at mid-depth of top beam on both sides.	not clear	Deterministic	Fairly match the experiment. Crack pattern shows diadonal crack in 45 and -45 directions.	No	1- concrete-steel bond stress-slip is modeled.
8	NRC	Li, Pires, Candra	2D plane stress	VecTor2	Smeared rotating crack model	Smeared reinforcement	Charlwood	nonlinear	concentrated displ is applied at mid-depth of top beam in middle	vertical constrained on the bottom of lower beam. Horizontal constrain only at CG.	Deterministic	crakcing is distributed in whole web, columns and beams. Majority is in the form of diagonal	they reported reduction in ductility by increasing the ASR expansion.	1- they acounted for three levels of ASR expasion (as lower, central and upper bounds). 2- they accounted for material degradation. 3) impact of maximum aggregate size is studied. 4) effect of linear and bilinear concrete softening is studied. 5) parametric analysis performed on material properties.
9	NRC-Japan	Kojima, Maruyama, Kodama, Jin, Nakamura, Nakano	3D (one-half the wall)	FINAS/STAR	quasi-orthogonal bi-directional model by Maekawa & Fukuura	reinforced concrete tension stiffness model with bond	Gocevski / Clayton et al.	nonlinear	applied displacement is distributed to all nodes at the center of the loading of top beam	bottom and sides of the lower beam is fixed.	Deterministic	Their model underestimate the experiment by ~20%.	They showed no further expansion after 260 until 1000. No meaningfull difference in capacity from 260 to 1000 days.	1- shell elements are verified by solid ones. 2) monotonic and cyclic test were performed.
10	Sweden	?	3D	Abaqus	damage plasticity	embeded steel bar	No real ASR model (themal expansion)	linear elastic	-	-	Parametric	They underestimate results for regular and ASR affected concrete in 260 and 1000 days under monotonic loading. For Cyclic load the results are even worth.	from 260 to 1000 there is no meaningfull differences.	They performed parametric analyses on the impact of different parameters: monotonic and cyclic loading, boundary condition, element type, concrete fracture energy, concrete compression side, concrete elastic stiffness, impact of vertical loading, shell element, reinforcement modeling, and confinment effect

1. Only one test was performed (1,000 days) and it is widely accepted (ACI, ASTM) that for an experiment to be representative it must be performed thrice.

2. There was some ambiguity as to what were the boundary conditions. This led to widely different assumptions to be made. Whereas this did not affect the ultimate load –displacement curve (calibrated), undoubtedly it resulted in different crack patterns and failure modes.

3. Selective record data was provided, and Colorado is not convinced that the load displacement is entirely

"correct". It was not explicitly explained how the displacement were recorded (i.e. where) and to the best of our knowledge, the capacity of the actuators was only 1,000 kN. Hence, past this limit it was one actuator pushing, and the other pulling. This can be extremely tricky experimentally from a control point of view.

4. Furthermore, the displacement was recorded as the difference between the top of the beam and the A frame connected to the lower one. This may explain why some analysts had a much softer response when they assumed (erroneously) that the displacement was recorded as an absolute one from the actuator's stroke measurement . Hence, it would have been desirable to have all the recorded data provided.

5. It was unfortunate that the AAR expansion at 1,000 days was nearly identical to the one at 260. This rendered the exercise moot. As practically any model ("right" or "wrong" could be tuned to achieve desirable results).

6. Last, but not least we were asked to make prediction of the wall response subjected to the same loading protocol [as the one from previous reported tests]. The load protocol is spelled out as :

   The rate of loading began with 0.005 mm/sec and was increased to a maximum of 0.15 mm/sec as cycles progressed. The first two cycles applied 0.2 mm lateral displacement in the plane of the wall in each direction and the subsequent cycles were at maximum displacements of 0.4, 0.6, 0.8, 1, 1.4, 1.8, 2, 2.5, 3, 4, 4.5, 5.5, 6, and 7 mm.

7. To our surprise the experimental curve for ASR B2 reported during our meeting was quite different.

   (a) Displacement feedback was measured with respect to the base, and not in absolute terms form the actuator stroke. (see above). Regretfully, this figure was not part of the problem statement.

   (b) The specimen was not loaded to the full 7 mm lateral displacement through 15 cycles as specified. It is clear that the test was terminated (why?) after a lateral displacement of only 2 mm and about 7 cycles. Given what is known about ASR there is no physical explanation for this sudden decrease in ductility other than "testing noise". For reference specimens REG A and B had nearly identical failure pattern/ductility.

   (c) Comparing the failure load –displacement curves for the three specimens, no trend emerges. B1 appears to be more ductile than A1, but less so than B2.

In summary, we remain convinced that this was an excellent exercise, yet clouded by: a) Quality and quantity of provided information; and b) nearly identical AAR expansion of A1 and B2 (from sample cylinders). Unfortunately, this was not conducive to use this exercise as a "validation" for the models[1].

Nevertheless, it was extremely interesting to compare and contrast models, and as such a tabulated summary is separately provided.

The authors have by now received an invitation to participate in the new ASCET2018 which is essentially the same as the 2017 one with the exception of the availability of additional measurements. They do not consider those clear/reliable enough to warrant their future participation.

---

[1]For an excellent discussion of validation/verification/calibration and others consult Thacker et al. (2004).